Post-seismic motion after 3 Chilean megathrust earthquakes: A clue for a linear asthenospheric viscosity

H. Boulze, L. Fleitout, E. Klein and C. Vigny
[1] Laboratoire de géologie - CNRS UMR 8538, École normale supérieure - PSL University, Paris, France

Supporting information

Contents

S1 Continuous GPS stations

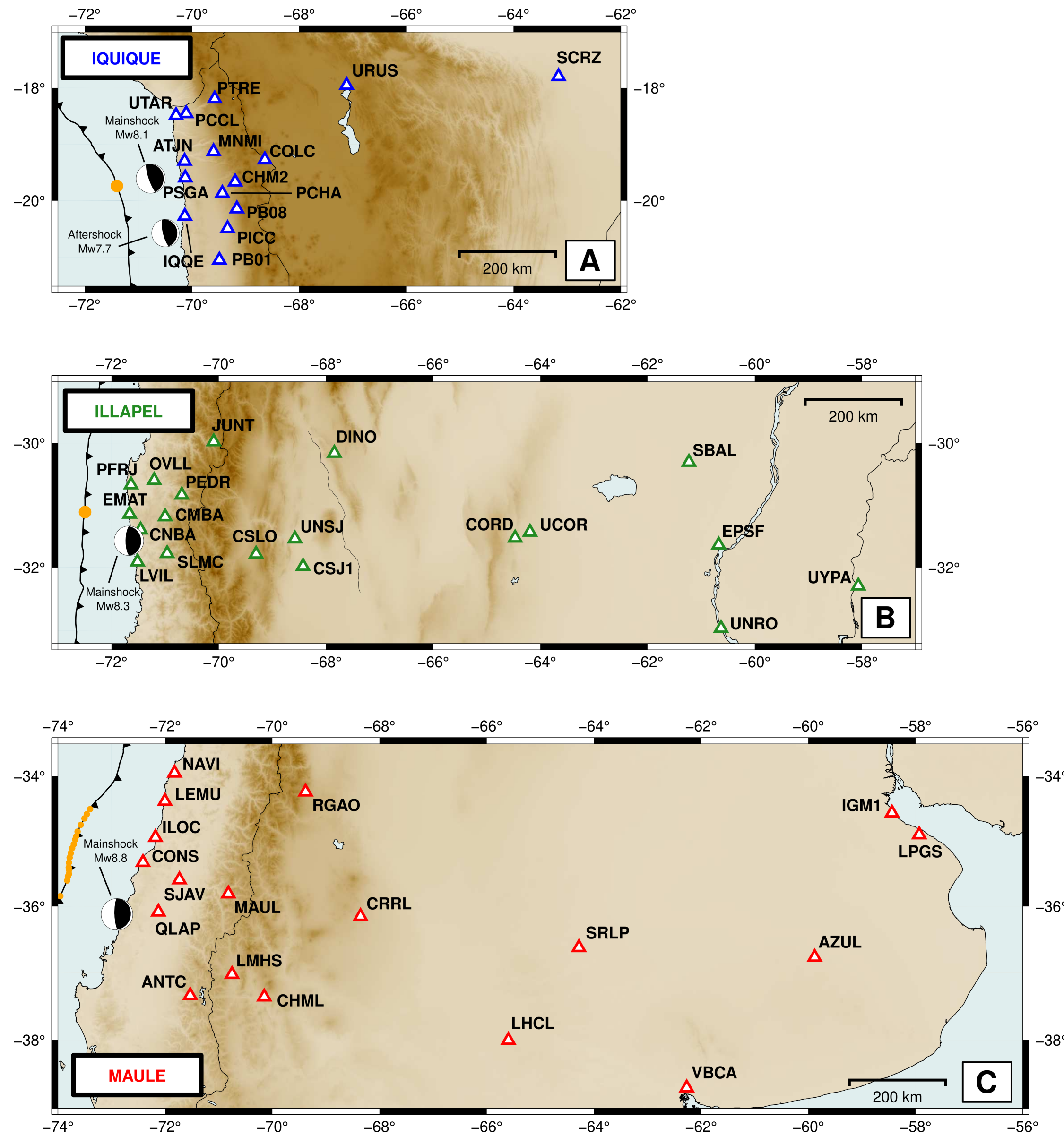

Figure S1: Continuous GPS stations used for Iquique (A), Illapel (B) and Maule (C) earthquakes. Distances from the trench are computed between orange points on the fault and the position of the stations. Several points are used for Maule because the co-seismic slip is more extended in latitude than for the other earthquakes: The distance from the trench is then computed between the station and the closest point.

S2 Details about the data analysis

S2.1 Correction from the pre-seismic trend

To estimate the cumulative post-seismic deformation, we remove a pre-seismic trend inverted by least squares. The period used to determine the trend is different for each station. In general, a good estimation requires more than 2.5 years of data to properly handle seasonal variations (Blewitt et Lavallée, 2002). However, due to the complexity of the GPS data (e.g. gaps, discontinuities, post-seismic signal before the earthquake), this amount of data can be difficult to obtain. For example, it is a delicate task to estimate a pre-seismic trend with more than 2.5 years for Illapel because some stations in the far-field are impacted by significant post-seismic deformation induced by the Maule earthquake.

Many stations have been installed after the Maule earthquake: CRRL, RGAO, LEMU, ILOC, LMHS, QLAP, NAVI, CHML. For these stations, we interpolate the Maule pre-seismic trend by using 34 continuous GPS stations located between $[-75^\circ E, -50^\circ E]$ in longitude and $[-45^\circ N, -30^\circ N]$ in latitude (Fig. S2).

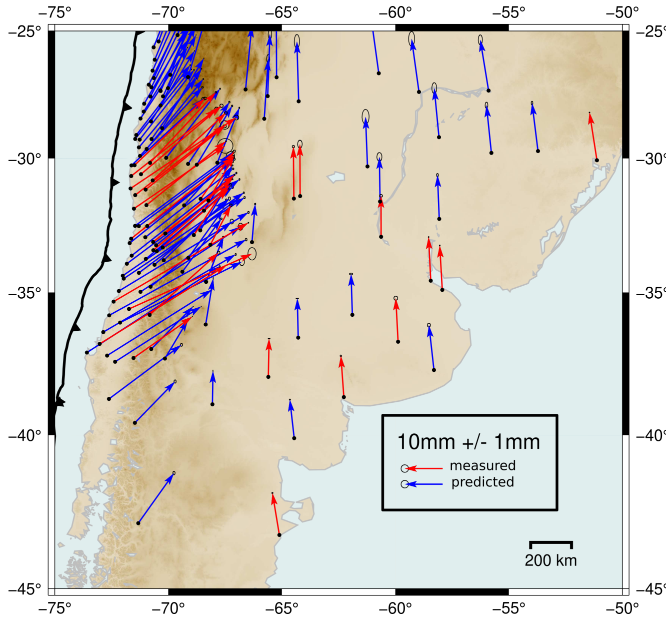

Figure S2: Interpolation of the pre-seismic velocity in ITRF2014 for stations installed after the Maule earthquake (blue vectors) or with less than 2 years of data before Maule.

S2.2 Co-seismic offset for Iquique earthquake

The Iquique earthquake is followed two days after by an important M_w 7.7 aftershock. In near and mid-fields, cGPS time-series clearly show a co-seismic offset due to the aftershock. To the south, the aftershock co-seismic offset is higher or of the same order as the mainshock offset(Fig. S3). Because we measure the post-seismic motion due to both earthquakes, we need to take into account the aftershock in *post/co ratios*. Thus, the Iquique co-seismic values that we use to plot the *post/co ratios* are based on the displacement at t_{EQ}+3days and takes into account the sum of the M_w 8.1 mainshock and the M_w 7.7 aftershock.

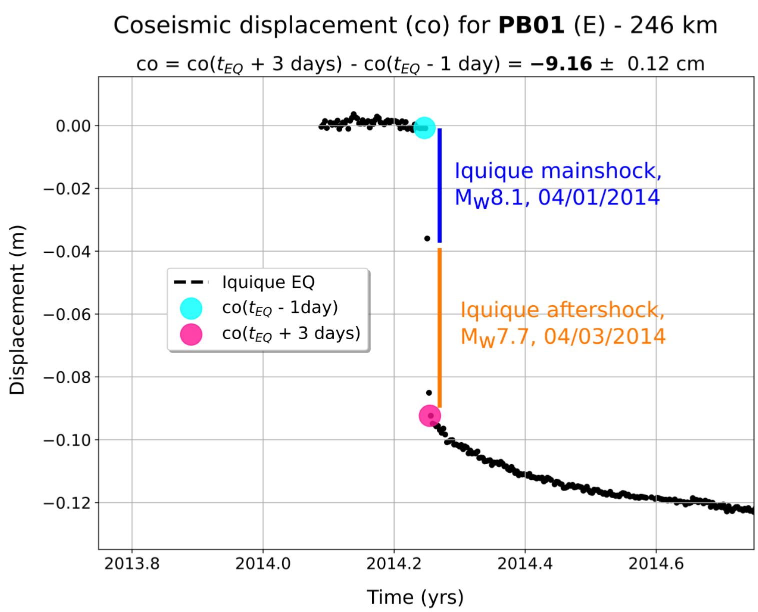

Figure S3: PB01 time-serie (E) where the co-seismic displacement induced by the Iquique M_w 7.7 aftershock is clearly visible and higher than that of the mainshock. PB01 is located closer to the aftershock than to the mainshock (see Fig. S1). t_{EQ} depicts the date of the earthquake.

S2.3 Uncertainties

- Pre-seismic trends: GPS velocity uncertainties depend on a combination of different kind of noises: white, flicker, random-walk, seasonal, ... Theses noises are variable, depending on the station monument quality (rocks, concrete, ...) and are also affected by data gaps and instrumental jumps. A complete quantification of the noise model of a particular data set is a difficult task, beyond the scope of this paper. A common way of estimating the uncertainty level of displacements inferred from noisy time series is to simply re-scale the formal uncertainty (which is well represented by the short term white noise) by a factor that range between 3 and 10 depending on the noise model and the station monuments behavior (e.g. Zhang *et al.*, 1997; Mao *et al.*, 1999; Bock et Melgar, 2016). Here we chose an intermediate factor of 5 which seemed appropriate to our stations and data processing: formal uncertainties re-scaled by 5, "match" long term noise at most stations. Re-scaling formal uncertainties is an oversimplification, but it is realistic and has the advantage of preserving relative uncertainties: some stations are better than others.

- Co-seismic offsets: The uncertainty σ_{co} associated with the value of the co-seismic offset is assumed equal to 2*RMS where RMS is the root mean square computed over the period $[t_{EQ} - 1yr, t_{EQ} + 1yr]$ with a 7 days sliding window. t_{EQ} depicts the date of the earthquake. When the co-seismic offset is computed from our finite element models, the uncertainty is set to 0.

- Cumulative post-seismic displacements: The uncertainty σ_{post} associated with the cumulative post-seismic displacement is set to two times the uncertainty on the pre-seismic velocity (see Section S2.1 for explanations): $\sigma_{post} = 2 \times \sigma_{pre}$.

- *post/co ratios*: The uncertainty $\sigma_{\frac{post}{co}}$ associated with the *post/co ratios* is then defined as below:

$$\sigma_{\frac{post}{co}} = \frac{post}{co} \times \sqrt{(\frac{\sigma_{co}}{co})^2 + (\frac{\sigma_{post}}{post})^2} \qquad \text{(Eq. S1)}$$

S3 Co-seismic offsets

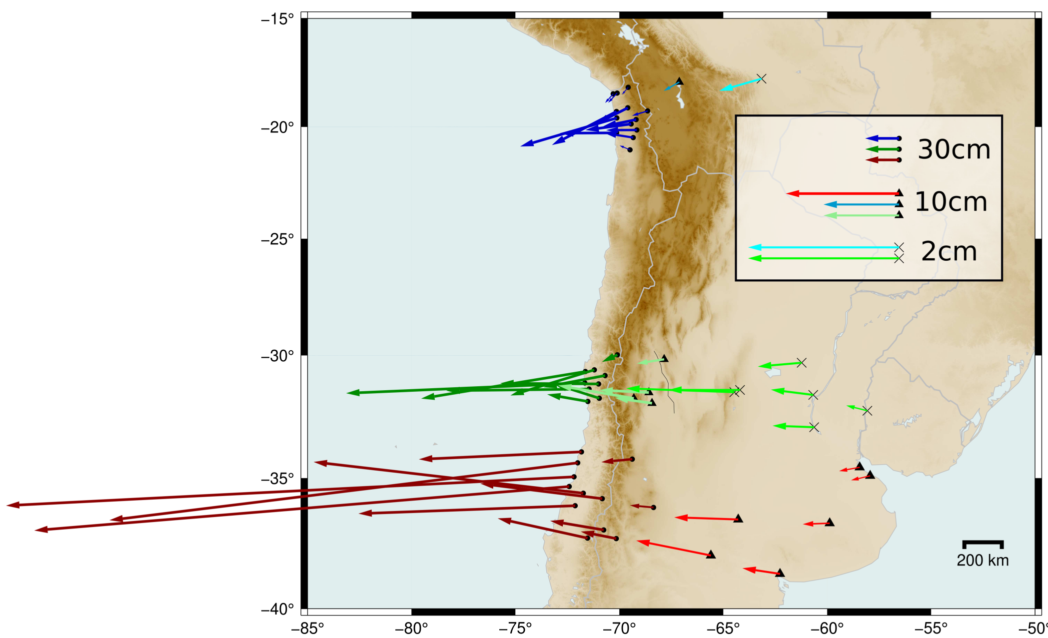

Figure S4: Co-seismic offsets (cm) for Maule (red), Iquique (blue) and Illapel (green) earthquakes. Note different scales for near-, mid- and far-fields.

For most stations, the co-seismic offset is measured on the time-series. But some stations did not record the earthquake (e.g. gaps, station installed shortly after the earthquake). In this case, we estimate the co-seismic offset from the co-seismic slip on the interface inverted in two previous studies: Klein *et al.* (2016) for Maule (CRRL, RGAO, LEMU, ILOC, LMHS, QLAP, NAVI, CHML) and Klein *et al.* (2017) for Illapel (EMAT, UCOR).

S4 Impact of afterslip

Near and mid-field post-seismic displacements are known to be highly impacted by afterslip during several years after the earthquake. Some studies have inferred long durations for afterslip, up to several decades (Suito et Freymueller, 2009), but recent studies relative to Maule (Klein *et al.*, 2016), Illapel (Xiang *et al.*, 2021) and Iquique (Hu *et al.*, 2021), indicate that most of the afterslip occurs during the two first years after the earthquakes.

In near and mid-field, even though the amplitudes of 2-5 years *post/co ratios* are smaller than for 0-5 years, they are still similar for the three earthquakes (Fig. S5). Understandably, uncertainties and scattering are larger when considering a time period over which displacements are smaller (years 2-5, Fig. S5-B versus years 0-2, Fig. S5-A). This effect is magnified in far-field (beyond 800-1000 km) where deformations become very small. The apparent difference in trends between Maule's (red symbols) and Illapel's ratios (green symbols) that shows in far field in Fig. S5-B is most probably an artefact. First, uncertainties are larger for Illapel smaller displacements and the scattering of the 3 points around 1100 km reflects this. Second, the perception of a decreasing trend is mostly driven by one point : the last one, which has the highest uncertainty. Last, Illapel's ratios are contaminated by the post-seismic deformation generated by the Maule earthquake, which occurred 5 years before. This contamination comes from the fact that during the period used to estimate the preseismic and the postseismic trend of Illapel, the signal coming from Maule is non negligible and not linear, at least according to the model of Klein *et al.* (2016). This affects the estimation of Illapel's post-seismic total displacement, yielding slightly smaller *post/co ratios*. This effect is present over both time periods, but highlighted for the 2-5yrs period (Fig. S5-B vs. S5-A).

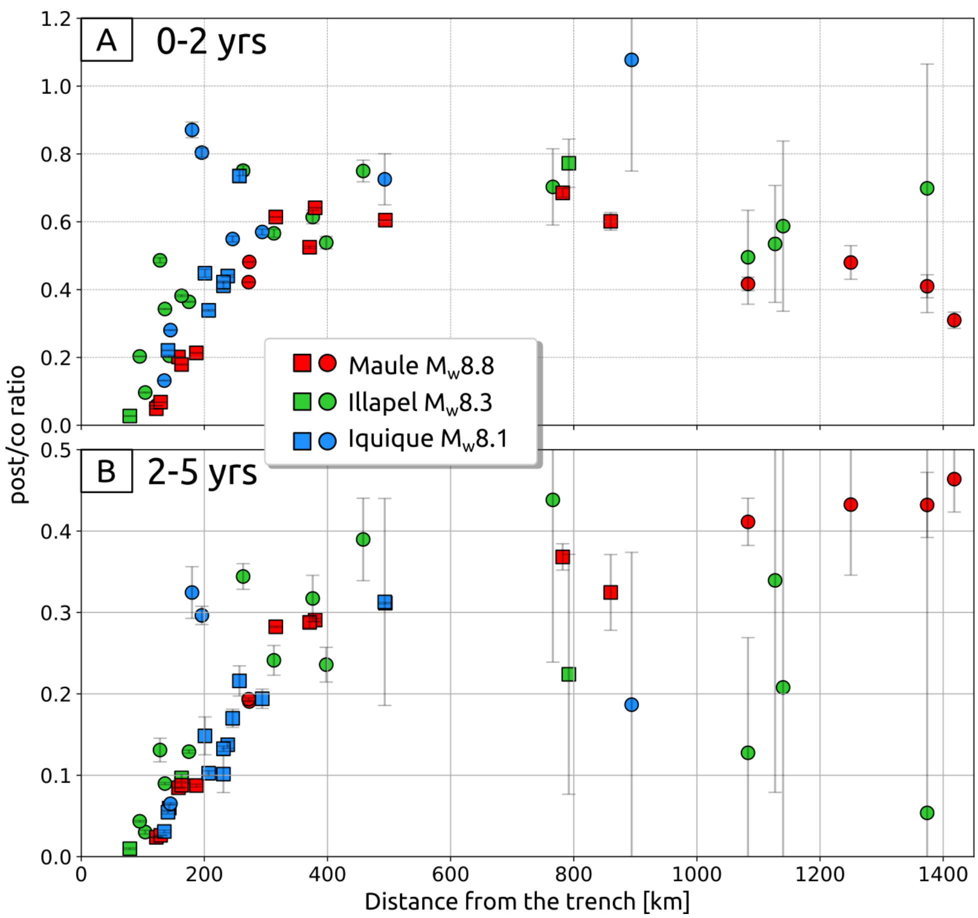

Figure S5: Evolution of the *post/co ratios* with distance from the trench over 0-2 yrs (A) and over 2-5 years (B). Dots depict observed displacements. Squares depict displacements for which some part of the time-serie was missing.

S5 Finite element mesh and models

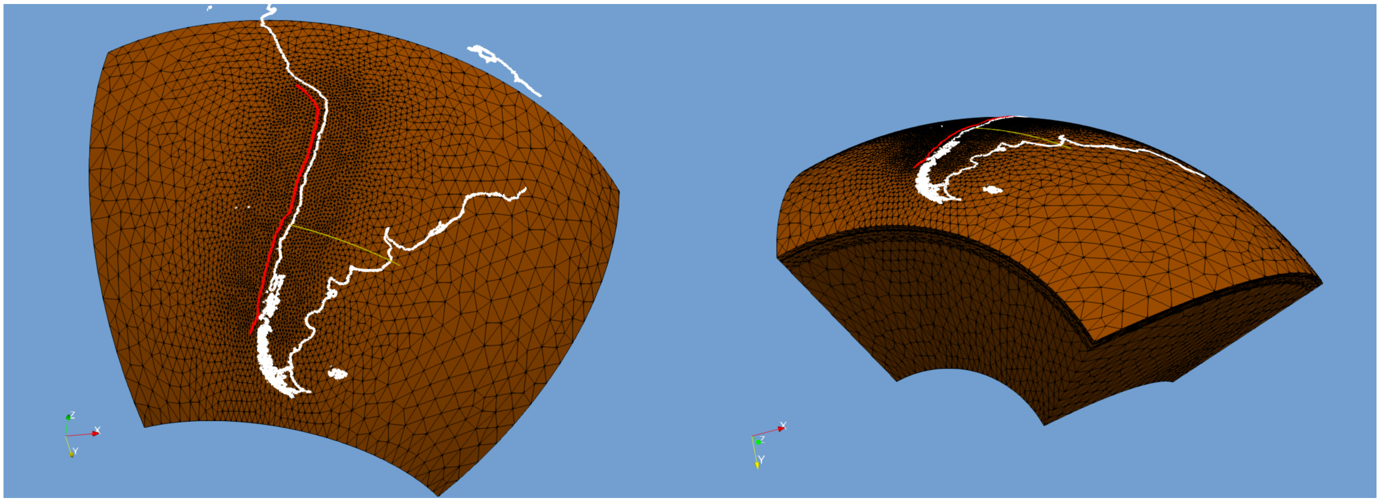

Figure S6: Finite element mesh developed by Klein *et al.* (2016) used in this paper. Coastlines are in white, the trench is in red and the profile P is in yellow.

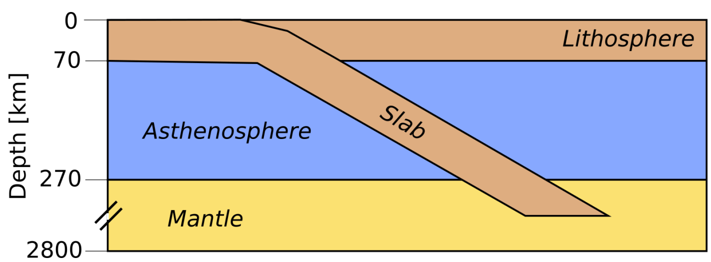

Figure S7: Sketch of a 2D section of the model.

For the numerical tests, we use the mesh developed by Klein *et al.* (2016) (Fig. S6). The geometry of the interface and the boundary conditions are exactly the same as in (Klein *et al.*, 2016). Contrary to Klein *et al.* (2016) who use Burgers rheology and lateral viscosity variations (wedge and channel), we use a uniform viscosity everywhere (Fig. S7). We also suppress the contribution of afterslip which is taken into account in Klein *et al.* (2016). According to seismic tomography of Celli *et al.* (2020), most of the GNSS stations we use are far from the thicker Brasilian craton. So, our simplistic model uses a lithosphere only 70 km thick and an asthenosphere extending from 70 to 270 km depth. Indeed, the seismic velocity at a depth of 100 km over the studied area is similar to that of the nearby old South-Atlantic ocean (Celli *et al.*, 2020). For the Newtonian case ($n = 1$), we use a linear-Maxwell rheology (no Burgers) with a viscosity of 4.75×10^{18} Pa.s for the asthenosphere. For the power-law case, we use Eq. 3 of the paper with $n = 3$. C is chosen to obtain approximately the same maximum *post/co ratio* for Maule earthquake, for the Newtonian and power-law cases: $C = 4.6 \times 10^{-29}$ Pa^{-3}.s^{-1}. For elastic parameters in the mantle and continental crust, a detailed description is provided in the supplements of Klein *et al.* (2016).

S6 The *post/co ratios* predicted by scaling laws and finite-element models

S6.1 Scaling laws

Computing the post-seismic deformation after an earthquake only involves an initial state, provided by the co-seismic slip and the visco-elastic mechanical equations i.e. the equilibrium equation and the constitutive visco-elastic equations. Note that the visco-elastic equations (equilibrium and Maxwell, Burgers or generalized Burgers constitutive equations) are all linear as long as the viscosities involved in the Maxwell or Burgers laws are linear. This justifies Eq. 1.

In the following sections, we develop the justification of Eq. 2 and Eq. 4.

S6.1.1 Justification of Eq. 2

The interplay between time and viscosity is well known in visco-elastic problems where the results are very often given uniquely as a function of a non-dimensional time (t/τ_M) where τ_M is the Maxwell time (Savage et Prescott, 1978). This simply derives from the visco-elastic constitutive equations. For a Maxwell visco-elastic solid, this equation writes, for Earthquake E2:

$$\frac{d\varepsilon_{ij}}{dt} = \frac{1}{9K}\delta_{ij}\frac{d\sigma_{kk}}{dt} + \frac{1}{2\mu}(\frac{d\tau_{ij}}{dt}) + \frac{1}{2\eta_2}(\tau_{ij}) \qquad \text{(Eq. S2)}$$

where we name ε_{ij} the elements of the strain tensor, σ_{ij} the elements of the full stress tensor and τ_{ij} the elements of the deviatoric stress tensor. K is the bulk modulus, μ the shear modulus and η_2 the viscosity at a given point in the mantle. To establish Eq. 2, we consider a same earthquake (same co-seismic slip) and same elastic properties (i.e. same initial stress and strain) but the viscosity for the case E1 is possibly spatially variable but everywhere multiplied by k with respect to E2 ($\eta_1 = k\eta_2$), where the rheology is here assumed to be linear i.e. η_1 and η_2 independent upon the deviatoric stress.

For Earthquake E1, the constitutive equation writes:

$$\frac{d\varepsilon_{ij}}{dt} = \frac{1}{9K}\delta_{ij}\frac{d\sigma_{kk}}{dt} + \frac{1}{2\mu}(\frac{d\tau_{ij}}{dt}) + \frac{1}{2\eta_1}(\tau_{ij}) \qquad \text{(Eq. S3)}$$

This viscoelastic equation is simply the time derivative of the Hooke's law where the term $\frac{1}{2\mu}(\frac{d\tau_{ij}}{dt})$ has been replaced by $\frac{1}{2\mu}(\frac{d\tau_{ij}}{dt}) + \frac{1}{2\eta_1}(\tau_{ij})$. It is equivalent to the equation used for example by Peltier (1974). Now in Eq. S3, we make a change of variables involving the time t: $t' = t/k$ Then Eq. S3 becomes exactly equal to Eq. S2 at any point in space except that t' replaces t.

The equations for solving the two problems are exactly the same and the initial and boundary conditions are the same. The solution of the two problems is then the same. Simply concerning the solution in the case of viscosity η_1, the post/co obtained for a time t' after solving equation S3 is in fact the solution for a 'real' time $t = kt$'. Note that the same change of variables would apply as well in the case of a Burgers rheology as long as the viscosities of the Kelvin-Voigt element are also in a ratio k.

S6.1.2 Justification of Eq. 4

Now let us consider two homothetic earthquakes but a same power-law rheology corresponding to Eq. 3. We assume that the co-seismic slip of E2 is λ times the slip of E1. There, the initial conditions differ as the initial strains and stresses for E2 are λ times the initial strains and stresses for E1. The viscosities are also different as they depend upon the amplitude of the deviatoric stress. The constitutive equation in a Maxwell case writes:

$$\frac{d\varepsilon_{ij}}{dt} = \frac{1}{9K}\delta_{ij}\frac{d\sigma_{kk}}{dt} + \frac{1}{2\mu}(\frac{d\tau_{ij}}{dt}) + (CJ_2(\bar{\bar{\sigma}})\tau_{ij}) \qquad \text{(Eq. S4)}$$

as $C.J_2(\bar{\bar{\sigma}})$ is equal to $\frac{1}{2\eta_{ef}}$ where η_{ef} is the effective viscosity in a power-law case. This equation is valid both for Earthquake 1 and Earthquake 2.

However, the related initial conditions are different. Concerning Earthquake E1, we make the following change of variables in Eq. S4: $(\epsilon_{ij})'_1 = \lambda(\epsilon_{ij})_1$, $(\sigma_{ij})'_1 = \lambda(\sigma_{ij})_1$ and $t' = t/\lambda^2$ where the subscript 1 refers to strain rates or stresses related to Earthquake 1. Then Eq. S4 becomes:

$$\frac{d(\varepsilon_{ij})'_1}{dt'} = \frac{1}{9K}\delta_{ij}\frac{d(\sigma_{kk})'_1}{dt'} + \frac{1}{2\mu}(\frac{d(\tau_{ij})'_1}{dt'}) + (CJ_2(\bar{\bar{\sigma}})'_1(\tau_{ij})'_1) \qquad \text{(Eq. S5)}$$

Eq. S5 is exactly the same as Eq. S4 but now, the initial condition in σ'_1 and ϵ'_1 is the same as the condition in σ and ϵ for Eq. S4 and earthquake E2. The two problems have then exactly the same solution. Simply, after getting the results by solving the problem for Earthquake E2 using equation S4, the displacements will have to be divided by λ and the times multiplied by λ^2 to get the solution for earthquake E1.

S6.2 Illustration in the case of two homothetic earthquakes: predicted time-series

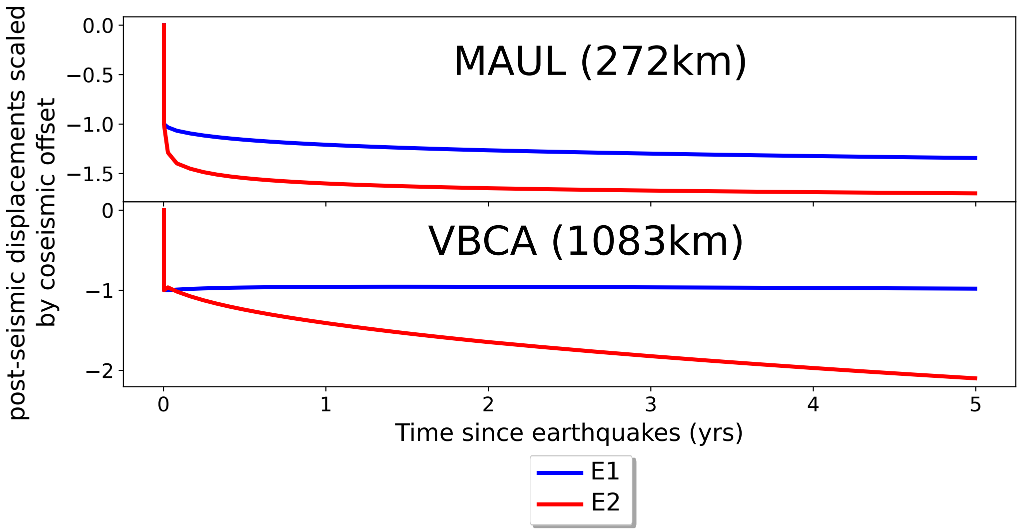

Figure S8: Co-seismic plus post-seismic displacements predicted by a model with a power-law viscosity at 2 cGPS stations for two fictive earthquakes: M_w 8.1 E1 from Fig. 3A (blue) and the fictive M_w 8.8 E2 from Fig. 3B (red). The time-series predicted by the power-law model differ strongly between large and smaller earthquakes. This can be set against the observations of Fig. 2B and Fig. 2C which show similar post/co time-series for earthquakes of very different magnitudes.

S6.3 von Mises stress in the asthenosphere predicted for two non-homothetic earthquakes

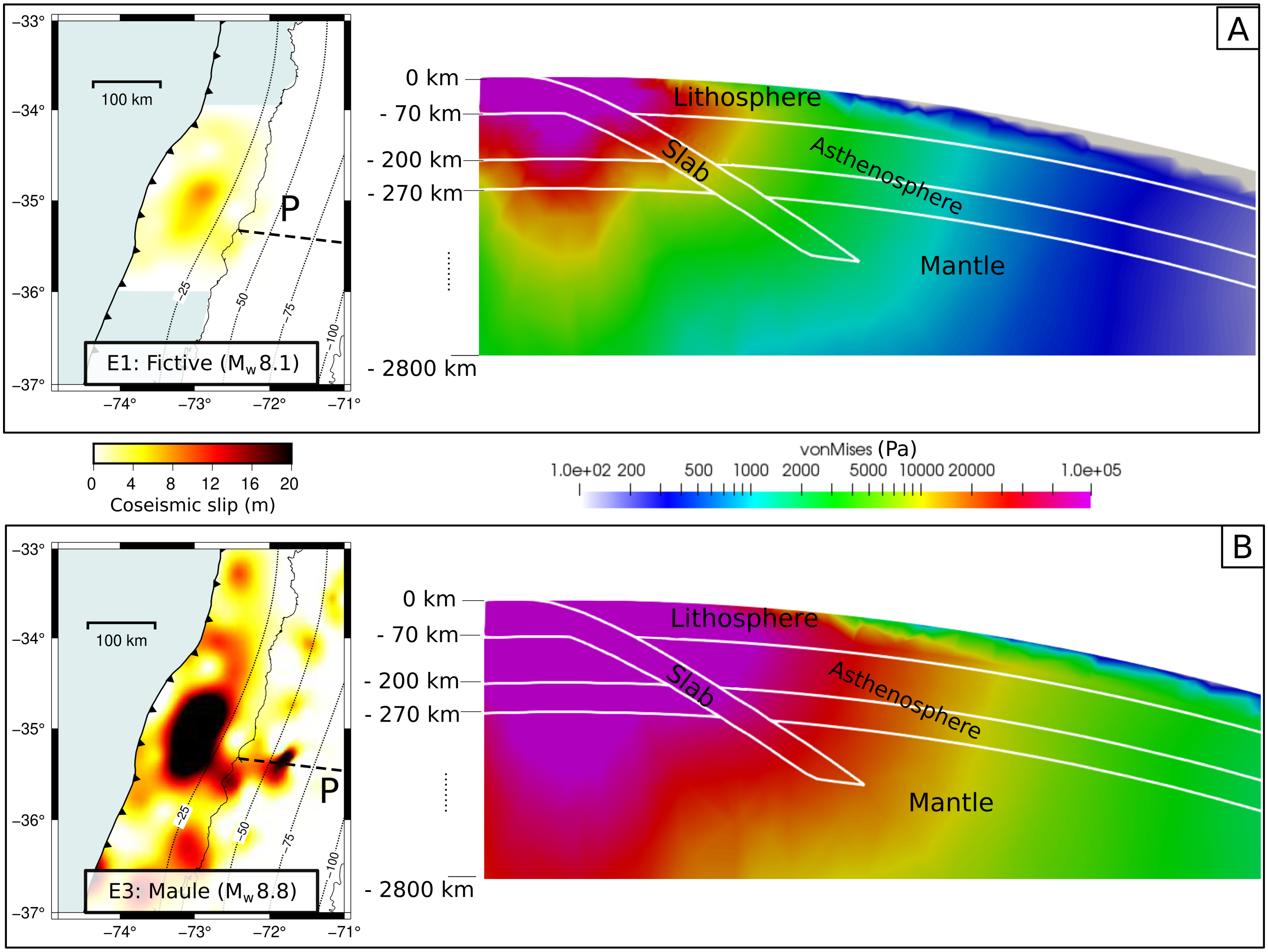

Figure S9: A-Fictive M_w 8.1 co-seismic slip distribution (left) and its associated von Mises stress (Pa) after the earthquake (right). B-Maule co-seismic slip distribution (Klein *et al.*, 2016) (left) and its associated von Mises stress (Pa) after the earthquake (right). A&B-von Mises stress is represented along the profile P. Note that the von Mises scale is logarithmic.

S7 Tables

Table 1: East component: Summary of the methods and values obtained to obtain the *post/co ratios* over 5 years. site: name of the continuous GPS station; lon/lat: longitude and latitude of the site; dist: distance from the trench of the site; EQ: name of the earthquake. Pre-seismic trend- period: amount of years before earthquake used to determine the pre-seismic velocity; method: data for least squares estimation and model for interpolation; value: value of the pre-seismic velocity; std: uncertainty associated with the velocity. Co-seismic- method: estimation made with data or model (finite element model); value: value of the co-seismic offset; std: uncertainty associated with the co-seismic offset. Post-seismic- method: estimation made with data or interp (interpolation); value: value of the cumulative post-seismic displacement; std: uncertainty associated with the cumulative post-seismic displacement.

site	lon (°)	lat (°)	dist (km)	EQ	Pre-seismic				Co-seismic			Post-seismic		
					method	period (yrs)	value (m)	std (m)	method	value (m)	std(m)	method	value (m)	std (m)
CMBA	-70.9990	-31.1882	143	Illapel	data	1.7067	0.0248	0.0009	data	-0.8670	0.0017	interp	-0.2293	0.0018
CNBA	-71.4580	-31.3982	104	Illapel	data	2.2067	0.0269	0.0008	data	-1.2594	0.0013	data	-0.1596	0.0015
CORD	-64.4701	-31.5284	766	Illapel	data	3.7067	0.0005	0.0007	data	-0.0143	0.0012	data	-0.0163	0.0014
CSJ1	-68.4272	-31.9805	398	Illapel	data	5.2067	0.0042	0.0003	data	-0.0494	0.0014	data	-0.0382	0.0005
CSLO	-69.3022	-31.7849	313	Illapel	data	2.2067	0.0124	0.0004	data	-0.1003	0.0014	data	-0.0809	0.0009
DINO	-67.8426	-30.1633	458	Illapel	data	2.2067	0.0059	0.0005	data	-0.0362	0.0009	data	-0.0413	0.0009
EMAT	-71.6627	-31.1467	79	Illapel	data	2.7067	0.0300	0.0005	model	-2.1048	0.0000	interp	-0.0781	0.0010
EPSF	-60.6721	-31.6399	1127	Illapel	data	3.5114	-0.0017	0.0004	data	-0.0056	0.0012	data	-0.0049	0.0007
JUNT	-70.0936	-29.9766	263	Illapel	data	3.2067	0.0161	0.0005	data	-0.1362	0.0023	data	-0.1492	0.0010
LVIL	-71.5139	-31.9092	128	Illapel	data	1.7067	0.0252	0.0013	data	-0.3594	0.0015	data	-0.2219	0.0026
OVLL	-71.2039	-30.6037	136	Illapel	data	3.7067	0.0217	0.0003	data	-0.7403	0.0014	data	-0.3203	0.0005
PEDR	-70.6891	-30.8390	175	Illapel	data	3.7067	0.0224	0.0003	data	-0.5436	0.0016	data	-0.2680	0.0005
PFRJ	-71.6354	-30.6747	95	Illapel	data	3.7067	0.0246	0.0004	data	-1.4480	0.0018	data	-0.3570	0.0007
SBAL	-61.2266	-30.3088	1083	Illapel	data	4.7054	-0.0016	0.0002	data	-0.0058	0.0015	data	-0.0036	0.0004
SLMC	-70.9628	-31.7770	163	Illapel	data	2.7067	0.0231	0.0004	data	-0.4042	0.0014	interp	-0.1934	0.0009
UCOR	-64.1935	-31.4349	792	Illapel	data	2.7067	-0.0010	0.0003	model	-0.0095	0.0000	interp	-0.0094	0.0007
UNRO	-60.6284	-32.9593	1140	Illapel	data	2.2067	-0.0021	0.0006	data	-0.0055	0.0014	data	-0.0044	0.0011
UNSJ	-68.5771	-31.5412	376	Illapel	data	2.2067	0.0085	0.0004	data	-0.0655	0.0015	data	-0.0610	0.0009
UYPA	-58.0672	-32.2912	1374	Illapel	data	2.9067	-0.0023	0.0004	data	-0.0028	0.0010	data	-0.0021	0.0008
ANTC	-71.5320	-37.3387	273	Maule	data	7.6569	0.0155	0.0001	data	-0.7922	0.0019	data	-0.5324	0.0001
AZUL	-59.8813	-36.7670	1250	Maule	data	2.4953	-0.0006	0.0005	data	-0.0237	0.0011	data	-0.0216	0.0010
CHML	-70.1501	-37.3591	380	Maule	model	0.0000	0.0061	0.0002	model	-0.3131	0.0000	interp	-0.2917	0.0003
CONS	-72.4121	-35.3309	122	Maule	data	5.8523	0.0356	0.0001	data	-4.7189	0.0017	data	-0.3866	0.0002
CRRL	-68.3543	-36.1527	494	Maule	model	0.0000	0.0020	0.0001	model	-0.2084	0.0000	interp	-0.1910	0.0001
IGM1	-58.4393	-34.5722	1374	Maule	data	6.1528	-0.0006	0.0001	data	-0.0181	0.0014	data	-0.0152	0.0002
ILOC	-72.1790	-34.9488	122	Maule	model	0.0000	0.0343	0.0004	model	-5.0102	0.0000	interp	-0.3647	0.0008
LEMU	-72.0034	-34.3910	129	Maule	model	0.0000	0.0320	0.0003	model	-4.1305	0.0000	interp	-0.3898	0.0006
LHCL	-65.5952	-38.0026	782	Maule	data	3.6542	0.0002	0.0003	data	-0.0659	0.0010	data	-0.0694	0.0005
LMHS	-70.7518	-37.0241	316	Maule	model	0.0000	0.0111	0.0001	model	-0.4729	0.0000	interp	-0.4239	0.0002
LPGS	-57.9323	-34.9067	1418	Maule	data	9.1542	-0.0007	0.0001	data	-0.0169	0.0012	data	-0.0130	0.0002
MAUL	-70.8214	-35.8096	272	Maule	data	3.0042	0.0182	0.0004	data	-1.0762	0.0026	data	-0.6624	0.0007
NAVI	-71.8246	-33.9527	158	Maule	model	0.0000	0.0297	0.0003	model	-1.4331	0.0000	interp	-0.4099	0.0006
QLAP	-72.1255	-36.0845	163	Maule	model	0.0000	0.0322	0.0014	model	-1.9119	0.0000	interp	-0.5103	0.0027
RGAO	-69.3798	-34.2455	371	Maule	model	0.0000	0.0103	0.0004	model	-0.2728	0.0000	interp	-0.2217	0.0009
SJAV	-71.7325	-35.5953	187	Maule	data	2.2542	0.0327	0.0010	data	-2.3784	0.0024	data	-0.7154	0.0021
SRLP	-64.2804	-36.6215	860	Maule	model	0.0000	-0.0002	0.0007	data	-0.0564	0.0011	data	-0.0522	0.0013
VBCA	-62.2692	-38.7008	1083	Maule	data	4.9528	-0.0008	0.0002	data	-0.0332	0.0013	data	-0.0275	0.0004
ATJN	-70.1368	-19.3008	141	Iquique	data	3.2466	0.0218	0.0003	data	-0.5694	0.0013	data	-0.1568	0.0006
CHM2	-69.1942	-19.6685	231	Iquique	data	0.9712	0.0183	0.0016	data	-0.2908	0.0011	interp	-0.1491	0.0033
COLC	-68.6386	-19.2762	294	Iquique	data	3.7466	0.0172	0.0004	data	-0.1380	0.0015	interp	-0.1054	0.0008
IQQE	-70.1317	-20.2735	145	Iquique	data	4.2466	0.0235	0.0002	data	-0.4999	0.0012	data	-0.1728	0.0003
MNMI	-69.5957	-19.1314	201	Iquique	data	1.4966	0.0181	0.0017	data	-0.2835	0.0014	data	-0.1692	0.0033
PB01	-69.4879	-21.0435	246	Iquique	data	4.2466	0.0241	0.0002	data	-0.0916	0.0012	interp	-0.0659	0.0005
PB08	-69.1610	-20.1430	238	Iquique	data	4.0466	0.0203	0.0003	data	-0.2698	0.0013	interp	-0.1558	0.0006
PCCL	-70.1067	-18.4577	196	Iquique	data	3.7466	0.0162	0.0002	data	-0.0789	0.0013	data	-0.0868	0.0004
PCHA	-69.4321	-19.8695	207	Iquique	data	4.2466	0.0204	0.0003	data	-0.4037	0.0013	interp	-0.1782	0.0006
PICC	-69.3346	-20.4898	231	Iquique	data	4.3466	0.0216	0.0002	data	-0.2474	0.0013	data	-0.1373	0.0004
PSGA	-70.1230	-19.5974	135	Iquique	data	3.7466	0.0231	0.0003	data	-0.8519	0.0014	interp	-0.1386	0.0007
PTRE	-69.5743	-18.1943	257	Iquique	data	3.2466	0.0099	0.0003	data	-0.0555	0.0011	interp	-0.0528	0.0005
SCRZ	-63.1597	-17.7968	894	Iquique	data	4.4013	-0.0006	0.0002	data	-0.0056	0.0016	data	-0.0071	0.0005
URUS	-67.1144	-17.9528	493	Iquique	data	1.7466	0.0071	0.0006	data	-0.0207	0.0013	interp	-0.0215	0.0013
UTAR	-70.2965	-18.4906	180	Iquique	data	3.0266	0.0173	0.0006	data	-0.0707	0.0014	data	-0.0845	0.0011

Table 2: North component: Summary of the methods and values obtained to obtain *post/co ratios* over 5 years. Same caption as Table S1

site	lon (°)	lat (°)	dist (km)	EQ	Pre-seismic				Co-seismic			Post-seismic		
					method	period (yrs)	value (m)	std (m)	method	value (m)	std(m)	method	value (m)	std (m)
CMBA	-70.9990	-31.1882	143	Illapel	data	1.9067	0.0207	0.0007	data	0.0055	0.0010	interp	-0.0052	0.0014
CNBA	-71.4580	-31.3982	104	Illapel	data	3.2067	0.0214	0.0004	data	-0.0139	0.0010	data	-0.0082	0.0008
CORD	-64.4701	-31.5284	766	Illapel	data	3.7067	0.0115	0.0006	data	0.0005	0.0012	data	-0.0041	0.0012
CSJ1	-68.4272	-31.9805	398	Illapel	data	4.3067	0.0115	0.0004	data	0.0071	0.0010	data	0.0067	0.0007
CSLO	-69.3022	-31.7849	313	Illapel	data	3.4067	0.0153	0.0002	data	0.0171	0.0011	data	0.0086	0.0004
DINO	-67.8426	-30.1633	458	Illapel	data	2.4067	0.0122	0.0004	data	-0.0056	0.0010	data	-0.0052	0.0007
EMAT	-71.6627	-31.1467	79	Illapel	data	1.7067	0.0222	0.0009	model	-0.0905	0.0000	interp	-0.0376	0.0018
EPSF	-60.6721	-31.6399	1127	Illapel	data	2.0067	0.0113	0.0008	data	0.0007	0.0009	data	0.0021	0.0015
JUNT	-70.0936	-29.9766	263	Illapel	data	3.2067	0.0180	0.0005	data	-0.0627	0.0021	data	-0.0587	0.0010
LVIL	-71.5139	-31.9092	128	Illapel	data	2.2067	0.0189	0.0008	data	0.0625	0.0011	data	-0.0654	0.0017
OVLL	-71.2039	-30.6037	136	Illapel	data	3.7067	0.0220	0.0002	data	-0.2261	0.0011	data	0.0064	0.0005
PEDR	-70.6891	-30.8390	175	Illapel	data	1.7067	0.0207	0.0007	data	-0.1029	0.0011	data	-0.0078	0.0015
PFRJ	-71.6354	-30.6747	95	Illapel	data	1.7067	0.0200	0.0019	data	-0.2386	0.0011	data	-0.0268	0.0038
SBAL	-61.2266	-30.3088	1083	Illapel	data	3.1067	0.0113	0.0003	data	-0.0005	0.0011	data	0.0011	0.0006
SLMC	-70.9628	-31.7770	163	Illapel	data	3.7067	0.0199	0.0003	data	0.1290	0.0010	interp	0.0028	0.0005
UCOR	-64.1935	-31.4349	792	Illapel	data	2.9067	0.0110	0.0003	model	-0.0000	0.0000	interp	-0.0000	0.0006
UNRO	-60.6284	-32.9593	1140	Illapel	data	2.7067	0.0114	0.0004	data	0.0002	0.0013	data	-0.0024	0.0008
UNSJ	-68.5771	-31.5412	376	Illapel	data	2.7067	0.0128	0.0003	data	0.0032	0.0013	data	0.0026	0.0006
UYPA	-58.0672	-32.2912	1374	Illapel	data	2.9067	0.0116	0.0003	data	0.0007	0.0009	data	-0.0013	0.0007
ANTC	-71.5320	-37.3387	273	Maule	data	7.6569	0.0109	0.0001	data	0.1743	0.0016	data	0.1099	0.0001
AZUL	-59.8813	-36.7670	1250	Maule	data	2.4953	0.0115	0.0005	data	-0.0008	0.0011	data	0.0024	0.0011
CHML	-70.1501	-37.3591	380	Maule	model	0.0000	0.0103	0.0005	model	0.0622	0.0000	interp	0.1168	0.0010
CONS	-72.4121	-35.3309	122	Maule	data	5.8523	0.0208	0.0001	data	-0.3879	0.0012	data	0.0257	0.0002
CRRL	-68.3543	-36.1527	494	Maule	model	0.0000	0.0122	0.0005	model	0.0192	0.0000	interp	0.0252	0.0010
IGM1	-58.4393	-34.5722	1374	Maule	data	6.1528	0.0115	0.0001	data	-0.0033	0.0012	data	-0.0026	0.0002
ILOC	-72.1790	-34.9488	122	Maule	model	0.0000	0.0208	0.0006	model	-0.2540	0.0000	interp	0.0704	0.0011
LEMU	-72.0034	-34.3910	129	Maule	model	0.0000	0.0219	0.0004	model	-0.5064	0.0000	interp	0.2407	0.0009
LHCL	-65.5952	-38.0026	782	Maule	data	8.1542	0.0101	0.0001	data	0.0132	0.0010	data	0.0197	0.0002
LMHS	-70.7518	-37.0241	316	Maule	model	0.0000	0.0112	0.0000	model	0.0801	0.0000	interp	0.0968	0.0001
LPGS	-57.9323	-34.9067	1418	Maule	data	6.1542	0.0117	0.0001	data	-0.0040	0.0010	data	0.0005	0.0003
MAUL	-70.8214	-35.8096	272	Maule	data	2.1542	0.0170	0.0006	data	0.1331	0.0016	data	0.1352	0.0012
NAVI	-71.8246	-33.9527	158	Maule	model	0.0000	0.0223	0.0004	model	-0.0658	0.0000	interp	0.0850	0.0009
QLAP	-72.1255	-36.0845	163	Maule	model	0.0000	0.0161	0.0020	model	-0.0701	0.0000	interp	0.0191	0.0040
RGAO	-69.3798	-34.2455	371	Maule	model	0.0000	0.0140	0.0004	model	-0.0258	0.0000	interp	-0.0198	0.0008
SJAV	-71.7325	-35.5953	187	Maule	data	1.6542	0.0146	0.0017	data	0.2758	0.0011	data	0.0644	0.0033
SRLP	-64.2804	-36.6215	860	Maule	model	0.0000	0.0104	0.0002	data	0.0019	0.0014	data	0.0105	0.0004
VBCA	-62.2692	-38.7008	1083	Maule	data	5.1528	0.0109	0.0002	data	0.0050	0.0013	interp	0.0087	0.0004
ATJN	-70.1368	-19.3008	141	Iquique	data	4.2466	0.0167	0.0002	data	-0.2959	0.0008	data	-0.0430	0.0003
CHM2	-69.1942	-19.6685	231	Iquique	data	0.9712	0.0172	0.0013	data	-0.0605	0.0007	interp	-0.0284	0.0026
COLC	-68.6386	-19.2762	294	Iquique	data	4.0466	0.0170	0.0003	data	-0.0421	0.0011	interp	-0.0261	0.0006
IQQE	-70.1317	-20.2735	145	Iquique	data	4.2466	0.0169	0.0001	data	-0.0027	0.0007	data	-0.0305	0.0002
MNMI	-69.5957	-19.1314	201	Iquique	data	4.2466	0.0182	0.0003	data	-0.1439	0.0010	data	-0.0618	0.0005
PB01	-69.4879	-21.0435	246	Iquique	data	4.0466	0.0171	0.0002	data	0.0381	0.0009	interp	0.0083	0.0004
PB08	-69.1610	-20.1430	238	Iquique	data	4.0466	0.0176	0.0003	data	-0.0016	0.0007	interp	-0.0139	0.0005
PCCL	-70.1067	-18.4577	196	Iquique	data	3.7466	0.0164	0.0002	data	-0.0855	0.0008	data	-0.0601	0.0003
PCHA	-69.4321	-19.8695	207	Iquique	data	4.2466	0.0175	0.0003	data	-0.0541	0.0009	interp	-0.0302	0.0005
PICC	-69.3346	-20.4898	231	Iquique	data	4.3466	0.0165	0.0002	data	0.0387	0.0007	data	-0.0017	0.0003
PSGA	-70.1230	-19.5974	135	Iquique	data	7.0068	0.0167	0.0001	data	-0.2514	0.0010	interp	-0.0467	0.0002
PTRE	-69.5743	-18.1943	257	Iquique	data	3.2466	0.0187	0.0002	data	-0.0645	0.0009	interp	-0.0692	0.0004
SCRZ	-63.1597	-17.7968	894	Iquique	data	4.4013	0.0126	0.0002	data	-0.0016	0.0012	data	-0.0053	0.0003
URUS	-67.1144	-17.9528	493	Iquique	data	4.1986	0.0150	0.0001	data	-0.0117	0.0008	interp	-0.0166	0.0003
UTAR	-70.2965	-18.4906	180	Iquique	data	3.0266	0.0152	0.0005	data	-0.0806	0.0009	data	-0.0615	0.0009

References

Blewitt, G. et Lavallée, D. (2002). Effect of annual signals on geodetic velocity. *Journal of Geophysical Research: Solid Earth*, 107(B7):ETG 9–1–ETG 9–11.

Bock, Y. et Melgar, D. (2016). Physical applications of GPS geodesy: a review. *Reports on Progress in Physics*, 79(10):106801.

Celli, N., Lebedev, S., Schaeffer, A., Ravenna, M. et Gaina, C. (2020). The upper mantle beneath the south atlantic ocean, south america and africa from waveform tomography with massive data sets. *Geophysical Journal International*, 221:178–204.

Hu, Z., Hu, Y. et Bodunde, S. S. (2021). Viscoelastic relaxation of the upper mantle and afterslip following the 2014 mw8.1 iquique earthquake. *Earthquake Research Advances*, 1(1):100002.

Klein, E., Fleitout, L., Vigny, C. et Garaud, J. (2016). Afterslip and viscoelastic relaxation model inferred from the large-scale post-seismic deformation following the 2010 Mw 8.8 Maule earthquake (Chile). *Geophysical Journal International*, 205(3):1455–1472.

Klein, E., Vigny, C., Fleitout, L., Grandin, R., Jolivet, R., Rivera, E. P. et Métois, M. (2017). A comprehensive analysis of the illapel 2015 mw8.3 earthquake from gps and insar data. *Earth and Planetary Science Letters*, 469:123–134.

Mao, A., Harrison, C. G. A. et Dixon, T. H. (1999). Noise in gps coordinate time series. *Journal of Geophysical Research: Solid Earth*, 104(B2):2797–2816.

Peltier, W. (1974). The impulse response of a maxwell earth. *Reviews of Geophysics*, 12(4):649–669.

Savage, J. C. et Prescott, W. H. (1978). Asthenosphere readjustment and the earthquake cycle. *Journal of Geophysical Research: Solid Earth*, 83(B7):3369–3376.

Suito, H. et Freymueller, J. T. (2009). A viscoelastic and afterslip postseismic deformation model for the 1964 alaska earthquake. *Journal of Geophysical Research: Solid Earth*, 114(B11).

Xiang, Y., Yue, J., Jiang, Z. et Xing, Y. (2021). Spatial-temporal properties of afterslip associated with the 2015 Mw 8.3 Illapel earthquake, Chile. *Earth, Planets and Space*, 73(1):27.

Zhang, J., Bock, Y., Johnson, H. O., Fang, P., Williams, S. D. P., Genrich, J. F., Wdowinski, S. et Behr, J. (1997). Southern california permanent gps geodetic array: Error analysis of daily position estimates and site velocities. *Journal of Geophysical Research*, 102:18035–18055.